High-Missing-Momentum Components in the ^{4}He$(e,e'p)^3$H Reaction

J. J. van Leeuwe,[1] H. P. Blok,[1,2] J. F. J. van den Brand,[3] H. J. Bulten,[3] G. E. Dodge,[1,2] R. Ent,[4] W. H. A. Hesselink,[1,2] E. Jans,[1,*] W. J. Kasdorp,[1] J. M. Laget,[5] L. Lapikás,[1] S. I. Nagorny,[1] C. J. G. Onderwater,[1,2] A. R. Pellegrino,[1,2] C. M. Spaltro,[1,2] J. J. M. Steijger,[1] R. Schiavilla,[4] J. A. Templon,[1,2] and O. Unal[3]

[1]*NIKHEF, P.O. Box 41882, 1009 DB Amsterdam, The Netherlands*

[2]*Vrije Universiteit Amsterdam, de Boelelaan 1081, 1081 HV Amsterdam, The Netherlands*

[3]*Department of Physics, University of Wisconsin, Madison, Wisconsin 53706*

[4]*TJNAF, Newport News, Virginia 23606, and Old Dominion University, Norfolk, Virginia 23529*

[5]*Service de Physique Nucléaire, CEA-Saclay, 91191 Gif-sur-Yvette Cedex, France*

(Received 2 July 1997)

The cross section of the ^{4}He$(e,e'p)^3$H reaction has been measured for missing momenta $220 \leq p_m \leq 690$ MeV/c to study high-momentum components of the nuclear wave function and the reaction mechanism for this transition. The zero predicted in the plane-wave impulse approximation (PWIA) cross section, due to the underlying pt momentum distribution, is found to be washed out. Three types of calculations indicate that this is caused by final-state interactions and contributions from two-body currents. The calculations reproduce the high p_m (600–690 MeV/c) data, although due to different ingredients in the models. [S0031-9007(98)05558-6]

PACS numbers: 21.45.+v, 21.30.–x, 24.10.Eq, 25.30.Fj

To obtain an adequate description of static properties of nuclei, nucleon-nucleon (NN) correlations have to be included in the nuclear wave function. Correlations are especially induced by the strong repulsive character of various components (spatial, spin-spin, tensor, etc.) of the NN interaction at small internucleon distances [1]. Calculations show that these NN correlations largely determine the high-momentum and high-energy components of the nuclear wave function [2]. Therefore the single-nucleon spectral function can provide relevant information for the study of correlations. Although most of the high-momentum strength is predicted to reside at large missing energies, i.e., in the breakup part of the spectral function, studies of specific transitions, e.g., to the ground state of the final nucleus, have clear advantages. Correlations also determine here the high-momentum behavior and a transition to a discrete final state allows for detailed calculations that account for final-state interactions (FSI), meson exchange currents (MEC), and isobar currents (IC). In this paper accurate experimental cross sections of the ^{4}He$(e,e'p)^3$H reaction are presented for missing-momentum (p_m) values as high as 690 MeV/c. The missing momentum is defined as $\mathbf{p}_m = \mathbf{q} - \mathbf{p}'$, where p' is the momentum of the knocked out proton, while the energy and momentum transferred by the virtual photon are denoted as ω and q, respectively. The motivation for the study of the ground state transition of the ^{4}He$(e,e'p)$ reaction is the fact that ^{4}He has an even larger central density (0.21 fm^{-3}) than heavy nuclei (0.17 fm^{-3}), and that realistic wave functions are available for ^{3}H and ^{4}He. In the plane-wave impulse approximation (PWIA) the $A(e,e'p)(A-1)$ cross section is proportional to the square of the amplitude $\langle p, A-1 \,|\, A\rangle$, the so-called $p(A-1)$ momentum distribution. Because of angular momentum and parity selection rules, only S waves contribute to the pt amplitude of the α particle. A characteristic feature of this momentum distribution is the prediction of a zero at $p_m \approx 450$ MeV/c. This zero is present only if correlations are included and its location depends on the NN interaction chosen [2]. However, a measured cross section will contain contributions from reaction mechanisms like FSI, MEC, and IC. Therefore this kinematic region, where the PWIA amplitude is very small, offers the opportunity to test models that account for these interaction effects [3–5]. Previous studies of the ^{4}He$(e,e'p)^3$H reaction, performed in quasielastic kinematics at NIKHEF [6] and Saclay [7], have shown that the p_m dependence of the cross sections up to 300 MeV/c is well described by microscopic calculations using realistic wave functions [4,5]. The calculated dependencies of the cross section on the three-momentum transfer and on the relative kinetic energy between the proton and triton were found to be in agreement within 10%–20%. This indicates that for $p_m \leq 300$ MeV/c and in the kinematic regime considered, the initial state as well as the microscopic treatment of FSI, MEC, and IC are well understood.

In a more recent experiment [8], performed at Saclay at a three-momentum transfer of 278 MeV/c in the dip region between the quasielastic and Δ-resonance peaks, the p_m dependence of the ^{4}He$(e,e'p)^3$H reaction was measured from 250 to 600 MeV/c. The low p_m ($\leq$300 MeV/c) data of this experiment were unexpectedly found to be at variance with theory. This only published measurement of the high p_m region can be improved in two aspects: (i) By choosing a higher momentum transfer effects beyond PWIA are expected to be reduced [5], and (ii) the statistical accuracy of the data can be improved considerably.

By employing a high-luminosity continuous electron beam and a large-acceptance proton detector, we have measured the $^4\mathrm{He}(e,e'p)^3\mathrm{H}$ cross section up to $p_m = 690$ MeV/c with good statistical accuracy. The electron beam was extracted from the Amsterdam Pulse Stretcher at NIKHEF [9], and had an energy of 525 MeV and duty factor of $\approx$50%. A cryogenic (15 K) high-pressure (4 MPa) cylindrical (i.d. = 5 cm) gas target was used [10]. The scattered electrons and the emitted protons were detected in the QDQ high-resolution magnetic spectrometer and the highly segmented scintillator detector HADRON4 [11], respectively. At its nominal distance from the target, HADRON4 has an in-plane and out-of-plane angular acceptance of $\pm 21°$, resulting in a solid angle of 550 msr. The angular resolution is 1° in plane and 2° out of plane. In combination with a 5.2 mm lead absorber in front of the detector, the proton energy acceptance is 67–195 MeV.

The choice of (ω, q) was dictated by the following considerations. First, the momentum transfer should be large enough to ensure quasielastic proton knockout. Second, the energy transfer was taken as small as possible to minimize the influence of the Δ resonance, with the constraint that at high p_m the kinetic energy of the emitted protons is still higher than the detection threshold of HADRON4. Therefore the angle and momentum of the scattered electrons were kept fixed throughout the experiment, resulting in a central transferred energy and momentum of 215 MeV and 401 MeV/c, respectively. The virtual-photon polarization was 0.63 and the invariant mass of the $(\gamma + \mathrm{p})$ system amounted to 1081 MeV/c^2. In four settings of the HADRON4 detector, emitted protons were detected at angles between 45° and 136° with respect to the beam, thus completely covering the missing-momentum range 220–690 MeV/c. An additional measurement of the low p_m region ($\leq$250 MeV/c) was performed in quasielastic kinematics at $(\omega, q) = (101\ \mathrm{MeV}, 408\ \mathrm{MeV}/c)$. These data [12] were in good agreement with calculations by Laget, by Schiavilla, and by Nagorny, as expected from the earlier measurements at low p_m mentioned above.

The response of the HADRON4 detector was calibrated using the continuous energy spectrum of proton singles events. The light measured in each scintillator was used for particle identification purposes, via the energy losses in successive scintillator layers, and for the determination of the kinetic energy of the proton. The live time of each detector element was accurately determined by feeding test pulses to the front-end electronics. The inefficiencies in track reconstruction and proton detection, due to hadronic interactions and multiple scattering, were calculated using the Monte Carlo code GEANT [13]. The simulations also produced estimates of the inefficiency arising from the discriminator thresholds. In the analysis these inefficiencies were corrected for on an event-by-event basis.

During several dedicated runs, in which elastically scattered electrons were detected in the QDQ and QDD spectrometers, the target thickness was determined using the known cross section for elastic scattering [14,15]. The target thickness was continuously monitored by recording, simultaneously with the $(e,e'p)$ coincidences, prescaled singles events in both spectrometers and HADRON4. These singles rates were linked to the count rates during the elastic scattering runs, in order to obtain the effective target thickness. This method resulted in an overall uncertainty in the target thickness of 2.5%.

Because of the limited vertex acceptance of the QDQ, the contribution of the target foils to the coincidence cross section was less than 0.1% at the chosen spectrometer angle. The contribution of accidental coincidences was subtracted from the data, which subsequently were converted to cross sections by dividing out the integrated luminosity and the detection volume in phase space. Finally, the data were corrected for radiative processes using the unfolding procedure described in Ref. [16]. The missing energy in an $(e,e'p)$ reaction is defined as $E_m = \omega - T_{p'} - T_{A-1}$, where the kinetic energy of the knocked out proton and recoiling $(A-1)$ system are denoted by $T_{p'}$ and T_{A-1}, respectively. Because of the experimental missing-energy resolution of $\approx$7 MeV (FWHM), the peak in the E_m spectrum, corresponding to the breakup of ^{4}He in a proton and a triton ($E_m = 19.8$ MeV), was not completely separated from the continuum formed by the contributions of the three-body $(pnd, E_m \geq 26.1\ \mathrm{MeV})$ and four-body ($E_m \geq 28.3$ MeV) breakup processes. The measured E_m spectra were fitted with the sum of a Gaussian and a phenomenological function for the continuum. The yield of the $^4\mathrm{He}(e,e'p)^3\mathrm{H}$ reaction for each p_m bin of 10 MeV/c was obtained by subtracting the continuum fit from the data, and integrating the remaining strength. The uncertainty in the fivefold differential cross section introduced by this procedure was estimated to be smaller than 3%. The overall systematical accuracy of the cross sections amounts to 5%.

In Fig. 1 the measured $^4\mathrm{He}(e,e'p)^3\mathrm{H}$ cross sections are shown as a function of p_m. The data decrease exponentially by more than 3 orders of magnitude with hardly a change of slope in the p_m region of the zero. The experimental cross sections are compared to three calculational methods developed by Laget, by Schiavilla, and by Nagorny. All three models use the wave functions of ^{2}H, ^{3}H, and ^{4}He that result from variational Monte Carlo calculations [17]. Laget and Schiavilla use wave functions obtained with the Urbana model-VII three-nucleon interaction and the Urbana or Argonne-v14 *NN* potential. The corresponding calculated ^{4}He binding energies [18] amount to 30.6 and 30.8 MeV, respectively (experimental value 28.3 MeV), and the zero in the pt momentum distribution is located at 490 MeV/c. Nagorny uses wave functions obtained with the Argonne-v18 two-nucleon and model-IX three-nucleon interaction [19]. This model predicts 27.8 MeV for the binding energy of the α particle, and 445 MeV/c for the zero in the pt momentum distribution. The calculations also differ in the way subnuclear

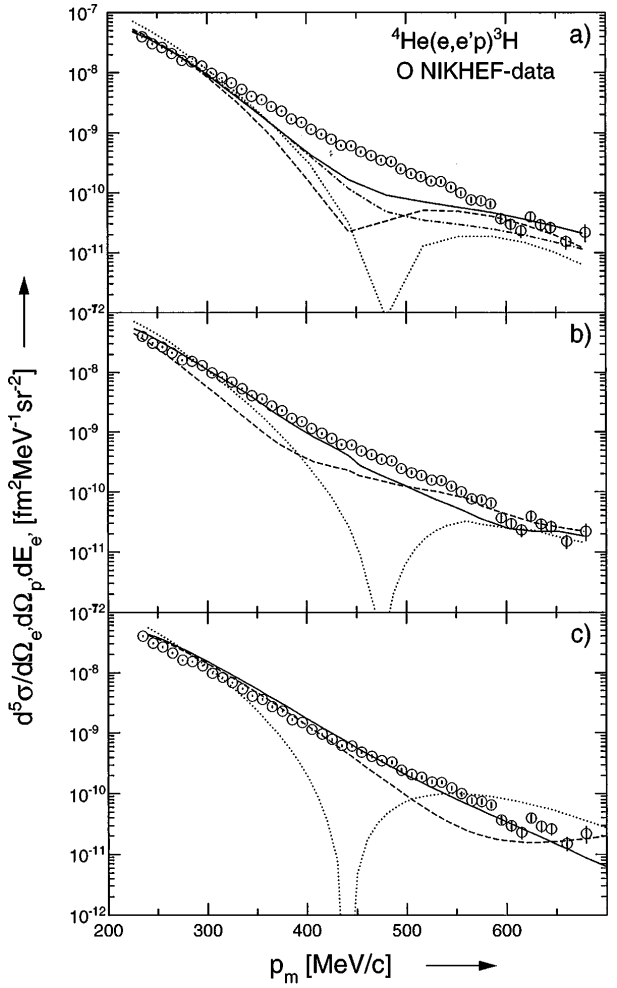

FIG. 1. Fivefold differential $^4\mathrm{He}(e,e'p)^3\mathrm{H}$ cross section as a function of the missing momentum for the $(\omega, q) = (215\ \mathrm{MeV}, 401\ \mathrm{MeV}/c)$ kinematics. The calculations in (a) were performed by Laget (dotted curve: PWIA, dashed: +FSI, dot-dashed: +two-body MEC, solid: +three-body MEC), in (b) by Schiavilla (dotted curve: PWIA, dashed: +FSI, solid: +two-body currents), and in (c) by Nagorny (dotted curve: PWIA, dashed: tree-type diagrams, solid: +one-loop diagrams).

effects (MEC and IC) and final-state interactions are treated. In the calculations by Laget [3,5] the processes contributing to the reaction amplitude are evaluated in a diagrammatic approach. FSI is treated using a single-rescattering diagram, while the effects of two- and three-body MEC are calculated by taking the most relevant processes into account. In Schiavilla's calculation [4] the pt scattering state is described by a correlated wave function. It consists of the product of the three-nucleon bound-state wave function and a distorted wave function for the outgoing proton, obtained from a complex optical potential containing a charge-exchange term. Central, spin, and tensor correlations between the proton and residual nucleons are included, to modify the pt cluster wave function at small internucleon distances, but not to change its behavior in the asymptotic region. The resulting wave function is then orthogonalized to the ^{4}He bound state (the so-called orthonormal-correlated state or OCS) and used to calculate the transition matrix elements relevant for the $^4\mathrm{He}(e,e'p)^3\mathrm{H}$ reaction. The charge and current operators, which provide a good description of the elastic form factors of few-body nuclei, contain one- and two-body terms, the latter constructed consistently with the NN interaction used. In the calculations by Nagorny [20,21] the electromagnetic field is included in the strongly interacting system in a fully relativistic and gauge invariant way. Two gauge invariant sets of tree-type and loop-type covariant diagrams are used. The tree-type set, consisting of the proton, triton, and ^{4}He poles and a contact diagram, obeys current conservation. The proton-pole diagram corresponds to the PWIA prediction, while the triton-pole diagram represents a crossing term. The diagram with the ^{4}He pole [3,22] accounts for the FSI part that corresponds to the pole piece of the $p^3\mathrm{H} \rightarrow p^3\mathrm{H}$ scattering T matrix [23]. The contact current, obtained from the Ward-Takahashi identities, provides gauge invariance on the level of the pole graphs and accounts partly for MEC effects [21]. In the full calculation also gauge invariant triangular and one-loop diagrams, which account for additional MEC and rescattering effects, are calculated. They account for the regular part of the $p^3\mathrm{H} \rightarrow p^3\mathrm{H}$ T matrix in S, P, and D waves, while fulfilling unitarity [21]. The half-off-shell T matrix for the $^1S_0$ wave was obtained in a separable form [24] using the unitarity condition and the $^4\mathrm{He} \rightarrow p^3\mathrm{H}$ vertex function. A renormalization has been applied to exclude "double counting" of the pole piece of the T matrix, which was already taken into account by the ^{4}He-pole diagram. Standard parametrizations are used for the electromagnetic form factors of the proton, ^{3}H, and ^{4}He [25], while the strong form factor in the $^4\mathrm{He} \rightarrow p^3\mathrm{H}$ vertex was calculated [21] from the overlap integral of the ^{3}H and ^{4}He wave functions.

In the following the data are compared to the results of the three calculations. The PWIA predictions (dotted curves in Figs. 1(a), 1(b), and 1(c) for the calculations by Laget, Schiavilla, and Nagorny, respectively), which represent the pt momentum distribution, are almost identical for $p_m \leq 300\ \mathrm{MeV}/c$. However, at higher missing momentum there are differences due to the different NN potentials used. The calculation presented in Fig. 1(c), which is performed with the $v18$ NN potential, has its minimum at a 45 MeV/c lower p_m value, while the strength in the second maximum is a factor of 4.5 larger than those of Figs. 1(a) and 1(b), where the $v14$ potential was used. All three full calculations, represented by the solid curves, give a good description of the data for missing momenta up to 300 MeV/c. In this region FSI effects slightly reduce the cross section. In the calculation by Laget MEC play a negligible role, while Schiavilla predicts a small increase due to the inclusion of MEC. In Nagorny's framework the effects of FSI and MEC cannot be disentangled.

The largest differences show up in the region $400 < p_m < 500\ \mathrm{MeV}/c$, where the cross section is dominantly

due to effects beyond PWIA, because of the zero in the pt momentum distribution. Here the data are at maximum underestimated by factors of 4 and 2 by the full calculations by Laget and Schiavilla, respectively. In this p_m region the contribution due to FSI [dashed curves in Figs. 1(a) and 1(b)] is considerably larger in Schiavilla's OCS method than in the diagrammatic approach of Laget. This is presumably due to the fact that in the OCS method rescattering is treated effectively to all orders by using an optical potential. Two-body MEC [dot-dashed and solid curves in Figs. 1(a) and 1(b), respectively] cause in both calculations an increase of the cross section for $p_m < 500$ MeV/c and a decrease above this value. Inclusion of three-body MEC by Laget [solid curve in Fig. 1(a)] increases the cross section for $p_m > 400$ MeV/c. A calculation by Nagorny in which only tree-type diagrams are taken into account [dashed curve in Fig. 1(c)] gives a fair account of the data. Here FSI and MEC effects are treated in a combined way. The full calculation, which also includes triangular and the one-loop diagrams [solid curve in Fig. 1(c)] and whose importance grows with increasing p_m, goes practically through the data.

All calculations give a good description of the cross sections for missing momenta between 600 and 700 MeV/c, but due to different ingredients in the models. Laget's full calculation is above the PWIA prediction. In Schiavilla's calculation the increase due to FSI gets largely canceled by two-body MEC. In Nagorny's calculation the full prediction is well below that of PWIA, but since he uses few-body wave functions that generate considerably more high-momentum components in the pt momentum distribution, the data are still well described.

In conclusion, we have measured the cross section of the ^{4}He$(e, e'p)^3$H reaction with high statistical accuracy over a large p_m region, including the part where PWIA calculations predict a zero in the cross section. The data decrease exponentially between $p_m = 220$ and 690 MeV/c with hardly a change of slope in the p_m region of the zero. Here, final-state interaction effects and two-body currents dominate the ^{4}He$(e, e'p)^3$H cross section in such a way that the zero in the PWIA prediction is almost completely washed out. The full calculations by Laget and Schiavilla underestimate the data in the intermediate missing-momentum range by a factor of 4 and 2, respectively. The calculation by Nagorny, which is based on a set of pole, contact, triangular, and one-loop diagrams, gives a good description of the data over the entire measured p_m interval. The few-body wave functions used in this latter approach are generated with the more recent $v18$ NN interaction. All three models give a fairly good account of the high p_m (600–690 MeV/c) data, but due to different ingredients in the calculations. The cross section is sensitive to the amount of high momentum components in the pt momentum distribution used, but firm conclusions can be drawn only when the contributions from mechanisms beyond PWIA can reliably be calculated over the complete p_m interval, including that of the zero.

Calculations indicate that it would be fruitful to separate experimentally the longitudinal, transverse, and longitudinal-transverse components of the ^{4}He$(e, e'p)^3$H cross section in the p_m region of the zero [5]. Since such an experiment requires a high-duty-factor electron beam of a few GeV as well as electron and proton detectors with good energy and angular resolution, it could be performed at TJNAF.

This work is part of the research program of the Foundation for Fundamental Research of Matter (FOM), which is financially supported by The Netherlands' Organisation for Advancement of Pure Research (NWO).

*To whom all correspondence should be addressed. Electronic address: eddy@nikhef.nl

[1] O. Benhar, V. R. Pandharipande, and S. C. Pieper, Rev. Mod. Phys. **65**, 817 (1993).
[2] H. Morita and T. Suzuki, Prog. Theor. Phys. **86**, 671 (1991).
[3] J. M. Laget, Can. J. Phys. **62**, 1046 (1984); J. M. Laget, in *New Vistas in Electronuclear Physics*, edited by E. Tomusiak *et al.* (Plenum, New York, 1986).
[4] R. Schiavilla, Phys. Rev. Lett. **65**, 835 (1990).
[5] J. M. Laget, Nucl. Phys. **A579**, 333 (1994).
[6] J. F. J. van den Brand *et al.*, Nucl. Phys. **A534**, 637 (1991).
[7] J. E. Ducret *et al.*, Nucl. Phys. **A556**, 373 (1993).
[8] J. M. Le Goff *et al.*, Phys. Rev. C **50**, 2278 (1994).
[9] P. K. A. de Witt Huberts, Nucl. Phys. **A553**, 845c (1993).
[10] O. Unal, Ph.D. thesis, University of Wisconsin, 1995 (unpublished).
[11] A. R. Pellegrino *et al.*, Nucl. Instrum. Methods Phys. Res. (to be published).
[12] J. J. van Leeuwe, Ph.D. thesis, University of Utrecht, 1996 (unpublished).
[13] GEANT: Detector Description and Simulation Tool, 1993, CERN Program Library W5013.
[14] C. R. Ottermann *et al.*, Nucl. Phys. **A436**, 688 (1985).
[15] J. S. McCarthy, I. Sick, and R. R. Whitney, Phys. Rev. C **15**, 1396 (1977).
[16] L. W. Mo and Y. S. Tsai, Rev. Mod. Phys. **41**, 205 (1969).
[17] R. Schiavilla, V. R. Pandharipande, and R. B. Wiringa, Nucl. Phys. **A449**, 219 (1986).
[18] A. Arriaga, V. R. Pandharipande, and R. B. Wiringa, Phys. Rev. C **52**, 2362 (1995).
[19] B. S. Pudliner *et al.*, Phys. Rev. C **56**, 1720 (1997).
[20] S. I. Nagorny *et al.*, Sov. J. Nucl. Phys. **49**, 465 (1989).
[21] S. I. Nagorny *et al.*, Sov. J. Nucl. Phys. **53**, 228 (1991).
[22] F. M. Renard *et al.*, Nuovo Cimento **38**, 565 (1965); **38**, 1688 (1965).
[23] S. I. Nagorny *et al.*, Phys. Lett. B **316**, 231 (1993).
[24] G. E. Brown and A. D. Jackson, *The Nucleon-Nucleon Interaction* (North-Holland, Amsterdam, 1976).
[25] A. A. Zayatz *et al.*, Sov. J. Nucl. Phys. **55**, 178 (1992).